# Co-emergence of Dirac and multi-Weyl Topological Excitations in Pnictide Antiperovskites

Wen Fong Goh and Warren E. Pickett

*Department of Physics, University of California, Davis CA 95616, USA*

(Dated: September 7, 2018)

The relatively unexplored family of pnictide-based antiperovskites has been shown to harbor prospects for topological phases. Using the example of $Ca_3BiP$, we demonstrate a cascade of phases as the initial cubic symmetry is broken successively. Initially a small gap $Z_2$ topological insulator, spin-orbit coupling leads to band re-ordering resulting in a topological semimetal phase. Compressive uniaxial (001) strain leads back to a small gap $Z_2$ topological insulator, with the expected gapless boundary modes. Tensile (001) strain leaves the system with a pair of Dirac points along $(0,0,\pm k_\circ)$ pinning the Fermi level, producing an unusual double meniscus of connected Fermi arcs on the (100) and (010) surfaces. Finally, breaking time-reversal symmetry by an applied Zeeman field produces a new phase with a pair of multi-Weyl nodes (massive or massless depending on direction, conventionally called semi-Dirac in two dimensional systems) simultaneous with a sister pair of Dirac modes along each $\pm k_z$ axis, combining to pin the Fermi level in the close vicinity of these varied single-particle excitations.

PACS numbers:

## I. INTRODUCTION

Topological bulk phases have a valence-conduction band inversion that must become disentangled at an interface to vacuum (*i.e.* at a surface), giving rise to topologically protected gapless, conducting surface states.[1] In three dimensions (3D), a $Z_2$ topological insulator (TI) is characterized by a $Z_2 = 0$ or $1$ topological invariant. Semimetals can also be classified by topological invariants, with the four-fold degenerate (including spin) Dirac point being the canonical example. Symmetry lowering has a strong impact. For a non-centrosymmetric (broken inversion symmetry (IS)) or magnetic (broken time reversal symmetry [TRS]) material, the effective low energy Hamiltonian for linear band crossing $\hbar v_F(\vec{\tau} \cdot \vec{k})$, where $\vec{\tau}$ are the Pauli matrices, has eigenvalues $E = \pm\hbar v_F|\vec{k}|$, with the sign providing the helicity of the Weyl particles.[2] There is an additional type of degeneracy, that of a conventional zero-gap semiconductor with quadratically touching bands that has no net topological character.

Intermediate between these degeneracies lie multi-Weyl points[3], from which dispersion proceeds as *either linear (massless) or quadratic (massive)* depending on direction. Multi-Weyl points are 3D generalizations of the semi-Dirac point in 2D that displays linear or quadratic dispersion depending on direction.[4,5]. Such points reflect a universe in which the form of the kinetic energy operator depends on direction. These points are protected by symmetry, however the semi-Dirac point in a broken TRS system can be driven by spin-orbit coupling to a Chern insulator phase.[6]

To date several structural classes of topological materials have been discovered or predicted, beginning with the topological insulator $Bi_{1-x}Sb_x$ alloys,[7] $Bi_2Se_3$ and related families.[8–12] Other materials, viz. $HgTe$[13], $\alpha$-Sn (gray tin) and halide perovskites[14], are not intrinsically topological but become so by tuning with strain to in-

duce a topological phase. Likewise, families of topological semimetals have been predicted and pursued.[15–19] Surface probes such as angle resolved photoemission spectroscopy (ARPES) and scanning tunneling microscopy (STM) are used to identify the corresponding topological surface states. In all of these systems, it is *sp* bands that provide the topological character.

The antiperovskite (APv) structure class of alkaline earth and pnictides compounds has been proposed to harbor potential topological insulating phases.[20,21] Our density functional theory based survey of the entire class of $3 \times 5 \times 5$ possible alkaline earth-pnictide APv compounds,[21] viz. $Ae_3Pn_APn_B$, where $Ae = $ Ca, Sr, Ba and $Pn_A, Pn_B = $ N, P, As, Sb, Bi, confirmed that some of these compounds in the assumed cubic structure host, or are very close to, non-trivial topological phases.

In this paper we choose a representative member of this new class and demonstrate that a sequence of symmetry lowering changes can propel a given compound through a cascade of phases that includes all of the above mentioned phases and into a new class in which both Dirac and multi-Weyl excitations lie in the close vicinity of the Fermi level, thus determining the transport and low-energy bulk excitations and providing connected Fermi arcs in the boundary spectrum.

## II. STRUCTURE, NOTATION, AND METHODS

This cubic APv structure (space group $Pm\bar{3}m$) has vertex-sharing $Ae_6Pn_B$ octahedra, with $Pn_A^{3+}$ ions in the interstitial A sites surrounded symmetrically by eight octahedra. Several nitrides in this class were surveyed by Niewa.[22] Our notation of elements $Ae$, $Pn_A$, and $Pn_B$ follows that of an antiperovskite with general chemical formula $X_3AB$, where the A cation is 12-fold cubo-octahedral coordinated and B is 6-fold coordinated by an

octahedron of $X$ cations. The central role of the anion was discussed previously; unlike in the oxide perovskites, the $A$ site rather than the $B$ site plays a central role in the electronic structure as it provides the uppermost valence bands that border the gap or invert with the conduction bands.

To obtain the electronic structure of the APv compounds $Ae_3Pn_APn_B$, the all-electron DFT method full-potential local orbital (FPLO) method,[23] was used with the generalized gradient approximation (GGA) exchange correlation of Perdew, Burke, and Ernzerhof (1996).[24] A dense $20 \times 20 \times 20$ $k$-mesh was used for self-consistency because of the delicate band overlap near $\Gamma$. Spin-orbit coupling (SOC) was included by using the fully relativistic four component Kohn-Sham-Dirac equation implemented in FPLO, without resorting to the intermediate scalar relativistic approximation.

Analysis of the band topology was done by calculating the $Z_2$ topological invariants following the Fu-Kane prescription, based on parity eigenvalues at the time-reversal invariant momenta (TRIM),[25] which are available from the FPLO code. About a dozen compounds have non-zero $Z_2$ invariants in the assumed cubic structure.[21] The surface spectrum was obtained by first obtaining the maximally-localized Wannier functions and corresponding hopping amplitudes.[26,27] A semi-infinite system is then constructed and the surface spectrum is calculated using the iterative surface Green's function method[28,29] with a tight binding hopping cut-off of 4 unit cells.



FIG. 1: Top panel: without SOC (blue) cubic $Ca_3BiP$ is a topological insulator with an anomalously small electron mass. SOC (red) re-orders the bands leaving a zero-gap semimetal. The large symbols denote Bi $6s$ character, demonstrating the $sp$ band re-ordering with SOC. Bottom panel: 5% tetragonal compressive strain in $Ca_3BiP$ results in a TI phase. The valence-conduction inversion energy is 0.28 eV.

## III. DISCUSSION OF RESULTS

Our computational survey[21] established that of two given pnictides, the stable structure always has the largest of the pair occupying the $A$ site. This anion provides the valence band maximum states; being the heaviest of the two pnictide atoms it provides the strongest SOC splitting, thus tending to promote inversion of valence and conduction bands and hence topological character. The lower conduction bands have $Ae$ $d$ orbital character. The cubic aPV compounds are mostly narrow gap semiconductors, with both conduction band minimum and valence band maximum occurring at $\Gamma$, giving SOC a central role in band inversion.

When band inversion occurs, $Pn$ $p$ orbitals with odd parity at $\Gamma$ are shifted above the lowest $a$ band which has even parity, due to $p$ eigenvalue splitting by SOC. Fig. 1 shows a rapid, almost abrupt, shift in the $s$ special character of Bi along $X-\Gamma-Z$. The three-fold cubic degeneracy at the $\Gamma$ point has to be connected by one conduction and two valence bands and results in a TSM state. By symmetry breaking, these TSM can be transformed into TI and DSM.
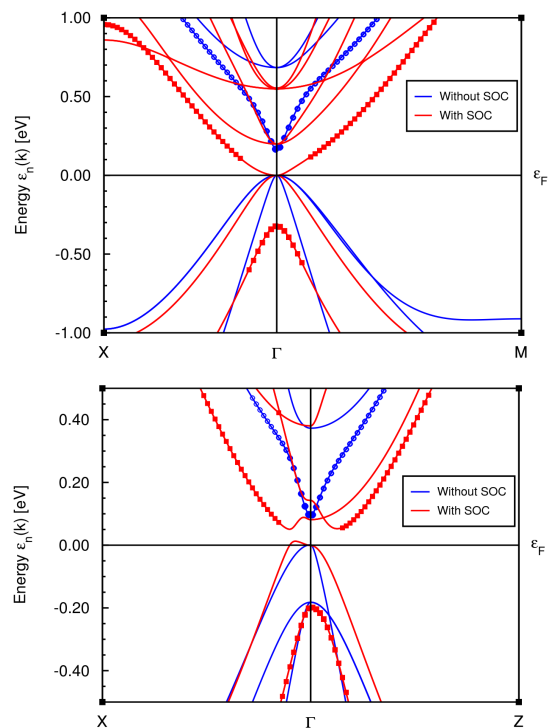
### A. Uniaxial compression

As a specific example we consider $Ca_3BiP$, one of the narrow gap APv semiconductors, as an example of a TI with $Z_2$ indices (1;000) before SOC is included. It has a calculated direct band gap of 0.16 eV at the $\Gamma$ point and the $p$ orbitals of the A site anion, Bi, lie at the bottom of the gap. SOC inverts the band ordering with an inversion energy of 0.28 eV, producing a topological band-touching semimetal due to degenerate $p_{3/2}$ states pinning the Fermi level. A compressive uniaxial strain in the range $1-7\%$ (the range we have studied) breaks the crystal symmetry while maintaining the inverted band ordering, and opens up a gap of 40 meV at the maximum strain, resulting in a TI phase. A representative band structure is shown in Fig. 1.

Topologically protected gapless surface states serve as direct confirmation of the topological bulk bands, and also serve directly as a bridge to experiment. The conducting character of these surface states is known to be robust against disorder, except when introduced by magnetic impurities (breaking TRS).[30] As shown in Fig. 2, both (001) and (100) surfaces have surface states crossing the bulk gap of 30 meV. The (001) surface shows bands
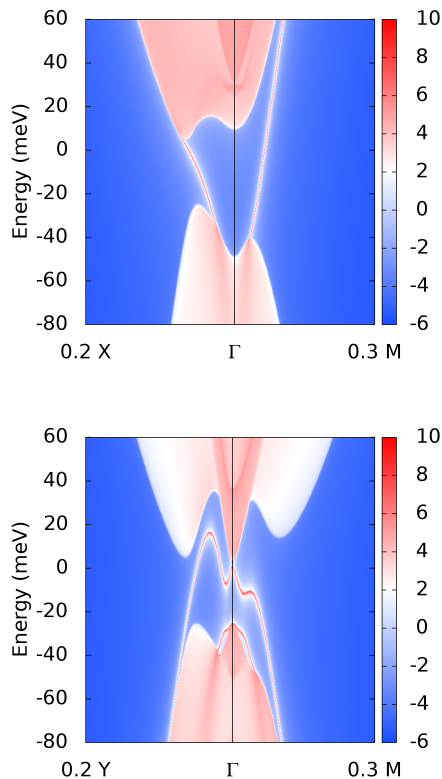
FIG. 2: Energy and momentum dependent spectral density of a semi-infinite crystal of (001)-compressed (5%) $Ca_3BiP$ terminated on (001) [top panel] and (100) [bottom panel] surfaces. Warmer colors represent higher intensity.

straightforwardly connecting the valence and conduction states, while the topological surface bands on the (100) surface incorporate a single Dirac point. These topological surface states are similar to those observed in $Bi_2Te_3$, $Sb_2Te_3$ and $Bi_2Se_3$.

### B. Uniaxial Expansion

Expansion of the lattice parameter $c$ of $Ca_3BiP$ by $1 - 5\%$ (the range we studied) also retains the band inverted ordering, but the different sign of eigenvalue splitting by SOC produces a different result. The surface spectrum displays a (two-fold) linear band crossing along $\Gamma - Z$ and gapped elsewhere as shown in Fig. 3. The band crossing point (4-fold degenerated including spins) is a signature of a quadruple Dirac point, and unavoidable as the bands have different irreducible representations, i.e. $\Gamma_6$ and $\Gamma_7$, as characterized and protected by the $C_{4v}$ rotational point group symmetry.

The (100) surface shows topological surface bands crossing the projected bulk band gap of about 20 meV (Fig. 4). The Fermi surface exhibits two topologically non-trivial Fermi arcs touching at the Dirac nodes
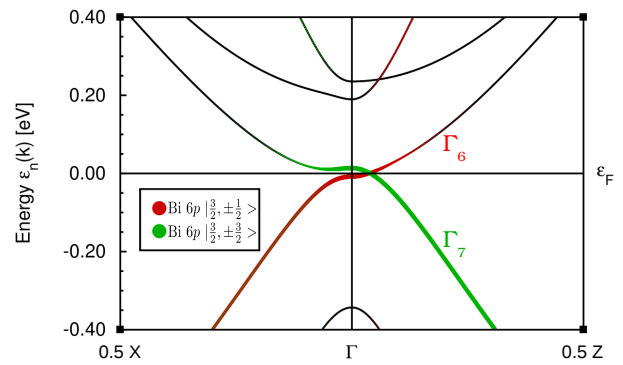


FIG. 3: Band structure of $Ca_3BiP$ with tensile strain of 1% along (001) shows a Dirac point at $\vec{k} = (0, 0, k_\circ)$, where $k_\circ = 0.022$ Å$^{-1}$. Around $k_\circ$, the bands have Bi $6p$ $|\frac{3}{2}, \pm\frac{1}{2} >$ and $|\frac{3}{2}, \pm\frac{3}{2} >$ characteristics.

$\vec{k} = (0, 0, \pm k_\circ)$ protected by both IS and TRS. This single pair of Fermi arcs connecting two Dirac points, like the Fermi arc connecting Weyl points in a WSM, is possible to exist, as a Dirac point can be treated as two Weyl points with opposite chirality, which in this case do not annihilate each other since the degeneracy is protected by the crystal symmetry. One notable property of the Fermi arc is that, ideally, electron density on the Fermi arc of one surface can sink through the bulk to the Fermi arc of the opposite surface, while eigenvalues remain continuous.

### C. Low energy description

An effective $4 \times 4$ Hamiltonian generalized from those used for $Na_3Bi$[31] and $Cd_3As_2$[32] can be adopted to describe the Dirac band crossing at $k_\circ$ in Fig. 3, with Bi $6p$ $|\frac{3}{2}, \pm\frac{1}{2} >$ and $|\frac{3}{2}, \pm\frac{3}{2} >$ states as the basis, in the order of $J_z = \frac{1}{2}, -\frac{3}{2}, -\frac{1}{2}, \frac{3}{2}$, after SOC. The Hamiltonian for the $C_4$ symmetry of $Ca_3BiP$ around $\Gamma$ reads, after (001) strain,

$$H_\Gamma(k) = \varepsilon_0(k) + \begin{pmatrix} M(k) & Ak_+ & 0 & 0 \\ Ak_- & -M(k) & 0 & 0 \\ 0 & 0 & M(k) & -Ak_- \\ 0 & 0 & -Ak_+ & -M(k) \end{pmatrix} \quad (1)$$

where the bands are $M(k) = M_0 - M_1 k_z^2 - M_2(k_x^2 + k_y^2)$ with negative constants to reproduce band inversion, $k_\pm = k_x \pm i k_y$ and $A$ provides the scale for coupling to uniaxial strain along $\hat{z}$. $k_\circ = \sqrt{M_0/M_1}$ gives the band crossing point along $\hat{z}$, and the dispersion around $k_\circ$ yields $E_{k_\circ} = \pm \sqrt{[2k_\circ \delta k_z - M_2(\delta k_x^2 + \delta k_y^2)]^2 + A^2(\delta k_x^2 + \delta k_y^2)}$.

*Time reversal symmetry breaking.* The Hamiltonian in Eq. 1 remains block-diagonal, containing two multi-Weyl Hamiltonian systems of opposite chirality. Symme-
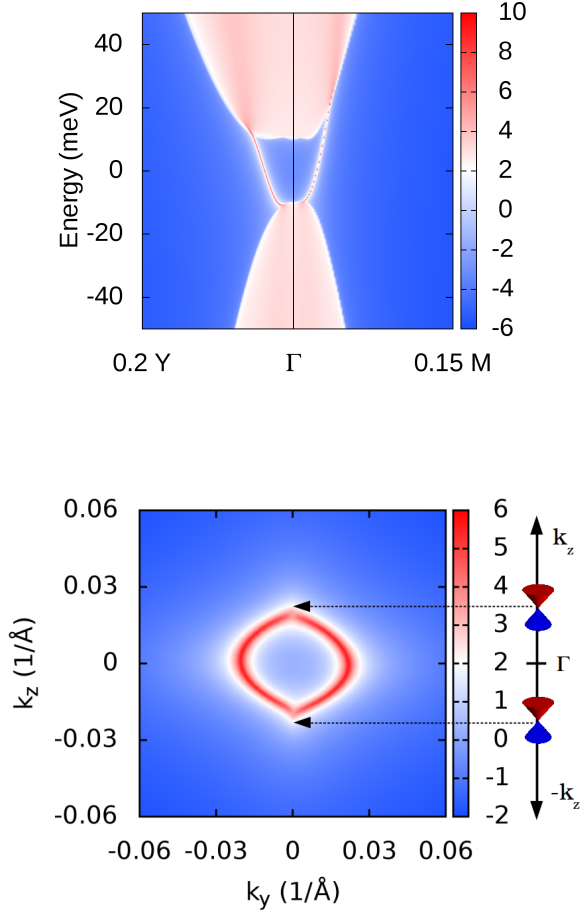
try can be broken further by violating IS or TR symmetry. Breaking IS is not an easy route, since the four-fold symmetry of Eq. 1 is to be preserved, otherwise it will open a gap and generate massive fermions. A simpler means is to apply an external Zeeman magnetic field $B$ coupling to the SOC basis sets, which preserves the crystal symmetry but breaks TRS,[33]

$$H_{Zeeman}(k) = H_{\Gamma}(k) + \begin{pmatrix} \Delta p_1 & 0 \\ 0 & \Delta p_2 \end{pmatrix} \otimes \sigma_z \quad (2)$$

where $\Delta p_{1,2} = \frac{1}{2} g_{1,2} \mu_0 B$ for Bi $6p \, |\frac{3}{2}, \pm\frac{1}{2} >$ and $|\frac{3}{2}, \pm\frac{3}{2} >$ states respectively. Eq. 2 can be block-diagonalized into $2 \times 2$ matrices,

$$H_{\pm}(k) = \left[ M(k) \pm \frac{(\Delta p_1 - \Delta p_2)}{2} \right] \sigma_z \pm \left[ \frac{(\Delta p_1 + \Delta p_2)}{2} \right] I \pm A(k_x \sigma_x + k_y \sigma_y) \quad (3)$$

The Weyl nodes are displaced to $\vec{k_\circ^*} = (0, 0, k_\circ^*)$, where $k_\circ^* = \sqrt{\frac{M_0}{M_1} \pm \frac{\Delta p_1 - \Delta p_2}{2M_1}}$. Expansion around $\vec{k_\circ^*}$ gives $E_{k_\circ^*} = \pm\sqrt{[2k_\circ^* \delta k_z - M_2(\delta k_x^2 + \delta k_y^2)]^2 + A^2(\delta k_x^2 + \delta k_y^2)} \pm (\Delta p_1 + \Delta p_2)/2$, where the Weyl Hamiltonians are decoupled along $\hat{z}$ into $k_\circ^*$ and shifted in energy by the average of the magnetic energies.

Fig. 5 illustrates the final spectrum for $B=24$ T ($\mu_B B \approx 1$ meV), for which the degeneracies are located at $k_{z,j} = \pm0.020\text{Å}^{-1}, \pm0.022\text{Å}^{-1}, \pm0.023\text{Å}^{-1}, \pm0.024\text{Å}^{-1}$. The former and latter lie at $E_F$ and occur for bands of opposite sign in $J_z$, while the middle two are for equal sign in $J_z$ occur above and below $E_F$. We observe that the nodes lying at $E_F$ are *multi-Weyl points*: linear dispersion along $k_z$ as shown in Fig. 5, and quadratic in the $k_x, k_y$ plane. A quantitative description in a tight binding scheme derived from maximally localized Wannier functions[26] is provided in the Supplemental Material. Our calculation on Na$_3$Bi also shows similar behavior.

The flow of the hybrid Wannier charge center (WCC) provides direct confirmation of the topological character. By constructing a closed 2D cut of the BZ containing a Weyl node, the evolution of the band sum of the hybrid WCCs around the closed cut can be calculated to determine the Weyl chirality.[34] Fig. 6 shows the evolution of the charge polarization of the two Weyl nodes at $E_F$, which indicates their corresponding chiralities $C_w = (-1, +1)$.

## IV. SUMMARY

In summary, we have shown that members of this class of APv materials can be driven into various topological phases by symmetry breaking. SOC, strain, and magnetic field can drive a cascade through a variety of topological phases. SOC drives or deepens band inversion by splitting the $Pn$ $p_{3/2}$ eigenvalues upward beyond



FIG. 4: Top panel: energy and momentum dependent spectral density of a semi-infinite crystal of (001)-expanded Ca$_3$BiP terminated on the (100) surface. Bottom panel: the (100) surface shows two half-circle Fermi arcs connecting projections of Dirac points along $\pm k_z$.
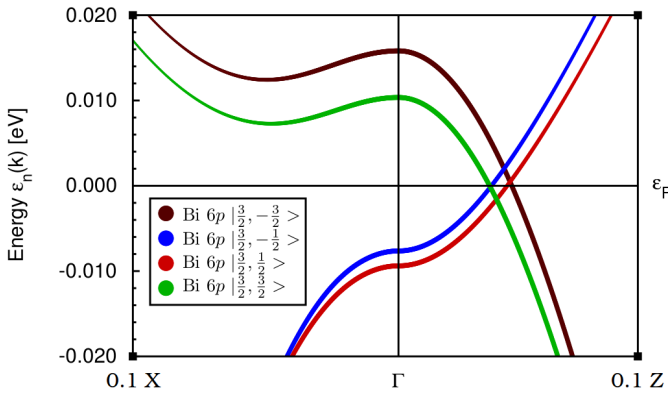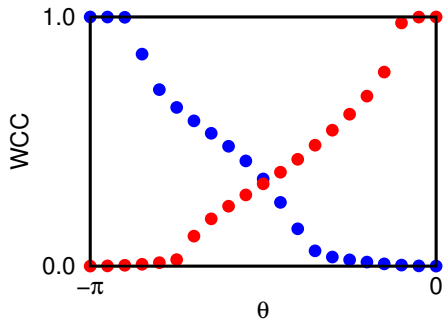


FIG. 5: Weyl nodes at $\vec{k_\circ^*} = (0, 0, k_\circ^*)$ under the external magnetic field of $B = 24$T. The bands are mostly split along $k_z$ and minimally in energy.

FIG. 6: The Wannier charge center (WCC) is computed for each loop at a constant azimuthal angle $\theta$ around a sphere surrounding Weyl points at $k_z = 0.020\text{Å}^{-1}$ (blue) and $0.024\text{Å}^{-1}$ (red). The change in the charge polarization for each loop from south ($\theta = -\pi$) to north ($\theta = 0$) for blue and red curves indicates $-1$ and $+1$ chiralities, respectively.

the $s$ conduction band at $\Gamma$, leaving a topological band-

touching semimetal. Uniaxial strain breaks the degeneracy and, if compressive, produces a topological insulator, while if tensile, gives a Dirac semimetal. At that point, application of a magnetic field breaks TRS and splits each Dirac node into a pair of Weyl nodes with opposite chirality, yielding a multi-Weyl points whose bounding projections are joined by Fermi arcs.

## V. ACKNOWLEDGMENTS

[1] M.Z. Hasan and C.L. Kane, *Colloquium*: Topological insulators, Rev. Mod. Phys. **82**, 3045 (2010).
[2] Wan, , , Savrasov, Phys. Rev. B **83**, 205101(2011).
[3] C. Fang, M. J. Gilbert, X. Dai, and B. A. Bernevig, Multi-Weyl Topological Semimetals Stabilized by Point Group Symmetry, Phys. Rev. Lett. **108**, 266802 (2012).
[4] V. Pardo and W. E. Pickett, Half-Metallic Semi-Dirac-Point Generated by Quantum Confinement in $TiO_2/VO_2$ Nanostructures, Phys. Rev. Lett. **102**, 166803 (2009).
[5] S Banerjee, R. R. P. Singh, V. Pardo, and W. E. Pickett, Tight-Binding Modeling and Low Energy Behavior of the Semi-Dirac Point, Phys. Rev. Lett. **103**, 016402 (2009).
[6] H. Huang, Z. Liu, H. Zhang, W. Duan, and D. Vanderbilt, Emergence of a Chern-insulating state from a semi-Dirac dispersion, Phys. Rev. B **92**, 161115(R) (2015).
[7] D. Hsieh, D. Qian, L. Wray, Y. Xia, Y.S. Hor, R.J. Cava, and M.Z. Hasan, A topological Dirac insulator in a quantum spin hall phase, Nature **452**, 970 (2008).
[8] H. Zhang, C.X. Liu, X.L. Qi, X. Dai, Z. Fang, and S.C. Zhang, Topological insulators in $Bi_2Se_3$, $Bi_2Te_3$ and $Sb_2Te_3$ with a single Dirac cone on the surface, Nat. Phys. **5**, 438 (2009).
[9] W. Zhang, R. Yu, H.J. Zhang, X. Dai, and Z. Fang, First-principles studies of the three-dimensional strong topological insulators $Bi_2Te_3$, $Bi_2Se_3$ and $Sb_2Te_3$, New J. Phys. **12**, 065013 (2010).
[10] O.V. Yazyev, J.E. Moore, and S.G. Louie, Spin polarization and transport of surface states in the topological insulators $Bi_2Se_3$ and $Bi_2Te_3$ from first principles, Phys. Rev. Lett. **105**, 266806 (2010).
[11] R. Li, Q. Xie, X. Cheng, D. Li, Y. Li, and X.Q. Chen, First-principles study of the large-gap three-dimensional topological insulators $M_3Bi_2$ ($M$ = Ca, Sr, Ba), Phys. Rev. B **92**, 205130 (2015).
[12] Y. Ando, Topological insulator materials, J. Phys. Soc. Jpn. **82**, 102001 (2013).
[13] J. Li *et al.*, Two-dimensional topological insulators with tunable band gaps: Single-layer HgTe and HgSe, Sci. Rep. **5**, 14115 (2015).
[14] H. Jin, J. Im, and A.J. Freeman, Topological insulator phase in halide perovskite structures, Phys. Rev. B **86**, 121102 (2012).
[15] H. Weng, X. Dai and Z. Fang, Topological semimetals predicted from first-principles calculations, J. Phys.: Condens. Matter **28**, 303001 (2016).
[16] R.Yu, H. Weng, Z. Fang, X. Dai, and X. Hu, Topological node-line semimetal and Dirac semimetal state in antiperovskite $Cu_3PdN$, Phys. Rev. Lett. **115**, 036807 (2015).
[17] S. Xu *et al.*, Discovery of a Weyl Fermion semimetal and topological Fermi arcs, Science **349**, 613 (2015).
[18] G. Xu, H.M. Weng, Z.J. Wang, X. Dai, and Z. Fang, Chern semimetal and the quantized anomalous Hall effect in $HgCr_2Se_4$, Phys. Rev. Lett. **107**, 186806 (2011).
[19] Y. Quan and W. E. Pickett, Single nodal loop of accidental degeneracies in minimal symmetry triclinic $CaAs_3$, Phys. Rev. Lett. **118**, 176402 (2017).
[20] Y. Sun, X.Q. Chen, S. Yunoki, D. Li, and Y. Li, New family of three-dimensional topological insulators with antiperovskite structure, Phys. Rev. Lett. **105**, 216406 (2010).
[21] W. F. Goh and W. E. Pickett, Survey of the class of isovalent antiperovskite alkaline-earth pnictide compounds, Phys. Rev. B **97**, 035202 (2018).
[22] R. Niewa, Alkaline-earth metal nitrides of the main-group elements: Crystal structures and properties of inverse perovskites, Z. Anorg. Allg. Chem. **639**, 1699 (2013).
[23] K. Koepernik and H. Eschrig, Full-potential nonorthogonal local-orbital minimum-basis band-structure scheme, Phys. Rev. B **59**, 1743 (1999).
[24] J.P. Perdew, K. Burke, and M. Ernzerhof, Generalized gradient approximation made simple, Phys. Rev. Lett. **77**, 3865 (1996).
[25] L. Fu and C.L. Kane, Topological insulators with inversion symmetry, Phys. Rev. B **76**, 045302 (2007).
[26] N. Marzari, A.A. Mostofi, J.R. Yates, I. Souza, and D.

Vanderbilt, Maximally localized Wannier functions: Theory and applications, Rev. Mod. Phys. **84**, 1419 (2012).

[27] P. Blaha, K. Schwarz, G. Madsen, D. Kvasnicka and J. Luitz, *WIEN2k*: An Augmented Plane Wave + Local Orbitals Program for Calculating Crystal Properties, (Karlheinz Schwarz, Techn. Universität Wien, Austria), 2001.

[28] M.P. Lopez Sancho, J.M. Lopez Sancho, J.M.L. Sancho and J. Rubio, Highly convergent schemes for the calculation of bulk and surface Green functions, J. Phys. F: Metal Physics **15**, 851 (1985).

[29] Q. Wu, S. Zhang, H.F. Song, M. Troyer and A.A. Soluyanov, WannierTools: An open-source software package for novel topological materials, Comput. Phys. Commun. (2017) https://doi.org/10.1016/j.cpc.2017.09.033.

[30] Y.L. Chen, J.H. Chu, J.G. Analytis, Z.K. Liu, K. Igarashi, H.H. Kuo, X.L. Qi, S.K. Mo, R.G. Moore, D.H. Lu, M. Hashimoto, T. Sasagawa, S.C. Zhang, I.R. Fisher, Z. Hussain and Z.X. Shen, Massive Dirac fermion on the surface of a magnetically doped topological insulator, Science **329**, 659 (2010).

[31] Z. Wang, Y. Sun, X.Q. Chen, C. Franchini, G. Xu, H. Weng, X. Dai and Z. Fang, Dirac semimetal and topological phase transitions in $A_3$Bi ($A$ = Na, K, Rb), Phys. Rev. B **85**, 195320 (2012).

[32] Z. Wang, H. Weng, Q. Wu, X. Dai and Z. Fang, Three-dimensional Dirac semimetal and quantum transport in $Cd_3As_2$, Phys. Rev. B **88**, 125427 (2013).

[33] H.Z. Lu and S.Q. Shen, Quantum transport in topological semimetals under magnetic fields, Front. Phys. **12**, 127201 (2017).

[34] D. Gresch, G. Autès, O.V. Yazyev, M. Troyer, D. Vanderbilt, B.A. Bernevig, and A.A. Soluyanov, $Z_2$Pack: Numerical implementation of hybrid Wannier centers for identifying topological materials, Phys. Rev. B **95**, 075146 (2017).